Spin-dependent transport through a single-walled carbon nanotube coupled to a ferromagnetic and a nonmagnetic metal electrode

L. W. Liu,[1,2] J. H. Fang,[1] L. Lu,[1] H. F. Yang,[1] A. Z. Jin,[1] and C. Z. Gu[1]
[1]*Institute of Physics, Chinese Academy of Sciences, Beijing 100080, People's Republic of China*
[2]*Department of Physics, Qiqihar University, Qiqihar 161006, People's Republic of China*
(Received 28 July 2006; revised manuscript received 7 November 2006; published 29 December 2006)

We report on transport measurements of an individual single-walled carbon nanotube (SWNT) coupled to a ferromagnetic and a nonmagnetic metal electrode. The low-temperature differential conductance shows a suppression of zero-bias conductance and Coulomb blockade oscillations, where the metallic SWNT behaves as a quantum dot. A marked hysteretic magnetoresistance is observed within the coercive region of the ferromagnetic metal film. The differential resistance has distinctly different values when the magnetization orientation is reversed. Our observed data suggest that the spin-split density of states lies within the SWNT quantum dot. We present an Anderson Hamiltonian to model the spin-polarized electron transport through the SWNT quantum dot with spin-split discrete levels, which supports the experimental observation.

DOI: 10.1103/PhysRevB.74.245429 PACS number(s): 73.63.Fg, 75.47.Pq, 72.25.Hg, 73.40.Ns

I. INTRODUCTION

Recently, there has been increasing interest in spin-dependent transport of carbon nanotubes coupled to ferromagnetic electrodes due to observations of hysteretic magnetoresistance (MR) along with their remarkable charge-dependent transport. Not only is the spin-related fundamental physics attractive, but also the promising applications in the emerging field of spin electronics whose central theme is that device resistance is controlled by means of the spin of the electrons rather than their charge.[1,2] Hysteretic MR behaviors have been observed in multiwalled[3–5] (MWNTs) and single-walled carbon nanotubes[6] (SWNTs) contacted by two ferromagnetic electrodes, in agreement with Jullière's model[7] and theoretical investigation,[8] where spins can be transported coherently over distances of around a few hundred nanometers in MWNTs and more than one micrometer in SWNTs, respectively. Moreover, hysteretic MR was not found[9] in a MWNT connected by one ferromagnetic contact (Co) and one metallic contact (Pt/Au) due to the absence of the spin-valve effect. However, a hysteretic MR of almost 100% and changes between positive and negative MR have recently been reported in a SWNT contacted by two ferromagnetic terminals.[10] The presence of MR in devices with a single ferromagnetic terminal was also reported in this work. In early work, positive and negative MR of about 30% in two-terminal ferromagnetic Co contacted by a MWNT were also reported.[11,12] These results call for a better understanding, going beyond Jullière's model, which fails to completely account for the large diversity in sign and magnitude of hysteretic MR, as well as MR appearing in a device with one ferromagnetic contact.

It has been demonstrated that finite-length SWNTs can act as one-dimensional quantum dots exhibiting Coulomb blockade and energy level quantization.[13,14] The combination of a spin-polarized electrode and a quantum dot is worth examination. In the combined system, the spin direction of electrons injected into the dot could be controlled by the external magnetic field, and electron transport would simultaneously be dominated by strong Coulomb interaction and the energy level structure in the quantum dot. More recently, the functional device of a spin transistor has been experimentally demonstrated, in which gate voltages can modulate the magnitude and sign of the hysteretic MR measured in carbon nanotube quantum dots contacted by two ferromagnetic electrodes.[15,16] The results of gate-controlled MR provide evidence for spin transport through carbon nanotubes. In addition, these experiments indicate that the influence of the energy spectrum of a carbon nanotube quantum dot on the transmission probability should not be negligible. In contrast, the simple Jullière model only involves the spin scattering in the ferromagnetic electrodes for which carbon nanotubes coupled to the ferromagnetic electrodes are considered as a spin waveguide with long spin coherence length.[3–6]

In this paper, we report on the observation of hysteretic MR with different values associated with the reversal of magnetization direction in a device of a SWNT coupled to a ferromagnetic and a nonmagnetic metallic electrode, where the SWNT enters the Coulomb blockade (CB) regime. We believe that the existence of the spin-split density of states (DOS) is responsible for the observed asymmetric MR. The relative change of asymmetric MR is up to approximately 7%, which is comparable to the tunneling MR results for a carbon nanotube coupled with two ferromagnetic terminals. This provides an interesting route for exploring carbon nanotubes in application of spin electronic devices.

Individual SWNTs were synthesized on a Si/SiO_2 substrate by chemical vapor deposition using methane as the feed stock with diameter ranging from 0.7 to 3 nm characterized by atomic force microscopy.[17] The degenerately doped silicon is used as a back-gate electrode and the thickness of the silicon dioxide layer is 500 nm. The SWNT was located relative to prefabricated Au alignment marks. A ferromagnetic, 50 nm colbalt (Co) film was deposited, and a nonmagnetic, 40 nm aluminum (Al)/10 nm gold (Au) film was then deposited on the SWNT fabricated by the multilevel lithograph technique using electron beam lithography (Raith 150). Figure 1 shows the scanning electron micrograph (SEM) of the hybrid device. Superconducting signatures were not found for the Au/Al electrodes by indepen-

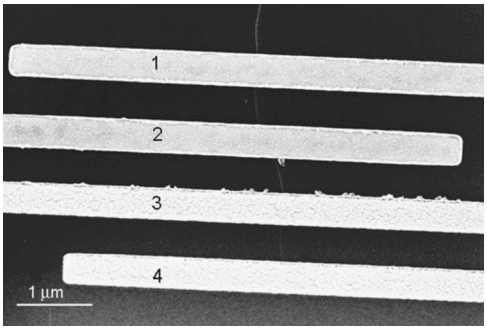

FIG. 1. SEM micrograph of the SWNT coupled to ferromagnetic Co electrodes represented by the numbers 1,2 and nonmagnetic metallic electrodes represented by the numbers 3,4. The electrode's width is approximately 350 nm and the separation of adjacent contacts is approximately 370 nm.

dent investigation. Instead, they behave only as nonmagnetic metal electrodes. At a bias voltage of 1 mV, the two-probe room temperature resistance was $R_{2,3} \sim 400\ \mathrm{k}\Omega$, and the current-voltage curve is symmetric even at low temperatures. This indicates that the SWNT was stably contacted with the ferromagnetic electrode (electrode 2) and the nonmagnetic electrode (electrode 3). Hereby, the following measurements are mainly carried out between electrodes 2 and 3. However, the value of $R_{2,3}$ is still larger than the intrinsic resistance of the individual SWNT and the symmetric current-voltage characteristic suggests that the two-terminal tunneling transport is dominant. The lack of dependence of the source-drain current on the gate voltages indicates that the SWNT is metallic. Figure 2 shows the temperature-dependent resistance $R_{2,3}$ of the SWNT from 0.35 to 300 K with a bias voltage of 1 mV. At low temperatures, the resistance rapidly rises, corresponding to highly suppressed conductance in the inset of Fig. 2. Figure 3 shows the differential conductance (dI/dV) curves between electrodes 2 and 3 at different temperatures. Zero-bias conductance suppression, which is the differential conductance dip centered at zero bias, is clearly observed below the temperature of 1 K. Figure 4 shows the oscillating differential conductance curve as a function of back-gate

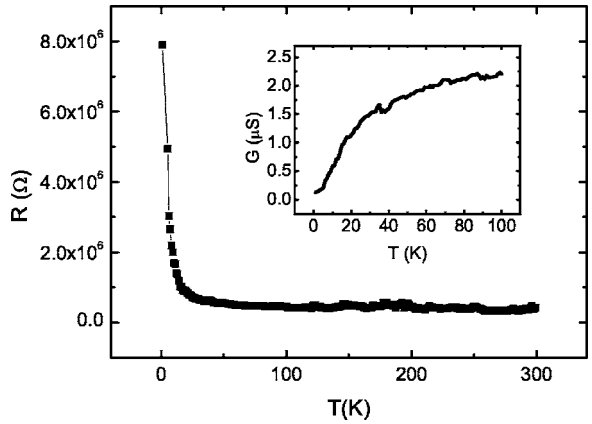

FIG. 2. Temperature-dependent resistance $R_{2,3}$ measured in two-probe configuration with the bias voltage of 1 mV from 0.35 to 300 K. The inset shows the corresponding temperature-dependent conductance from 1 to 100 K.

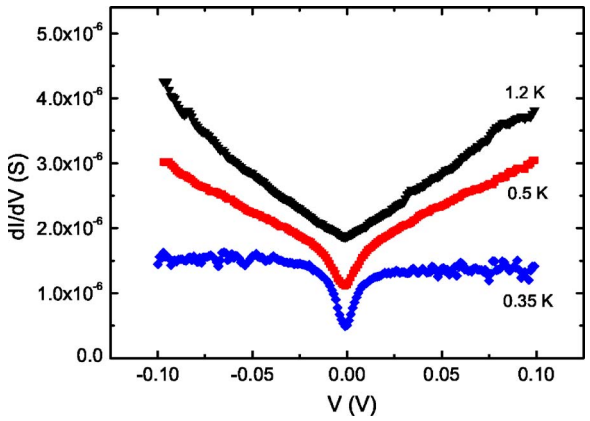

FIG. 3. (Color online) The differential conductance dI/dV as a function of the bias voltages at 0.35, 0.5, and 1.2 K between electrodes 2 and 3. The curve displays a pronounced suppression of zero-bias conductance below 1 K.

voltage at various temperatures with a bias voltage of 5 mV. From conductances lower than $e^2/\hbar$ [38.8 μS or $(25.8\ \mathrm{k}\Omega)^{-1}$], and the dependence of their average values on the bias voltage and temperature, we conclude that these periodic oscillations do not result from Fabry-Pérot interference,[18] but from Coulomb blockade oscillations. Thus, transport is dominated by Coulomb blockade in the low-temperature regime and there exists tunnel resistance at the contacts between the SWNT and the electrodes. The SWNT behaves as a quantum dot resulting in the low-temperature suppression of conductance. In Fig. 3, we perform the analysis using the CB theory;[6] the threshold voltage of conductance suppression is about 13 mV, which is consistent with the theoretical estimate $V_{th}=(U_c+\Delta E)$, where $U_c \approx 5\ \mathrm{mV}/[L(\mu\mathrm{m})]$ and $\Delta E \approx 1.0\ \mathrm{meV}/[L(\mu\mathrm{m})]$ are the single-electron charging energy and level spacing, respectively.[19] Taking the contact separation between electrodes 2 and 3 $L \sim 370$ nm, we estimate $V_{th} \sim 16$ mV.

Low-temperature differential reistance (dV/dI) measurements between electrodes 2 and 3 employed an ac lock-in technique with the magnetic field from a superconducting

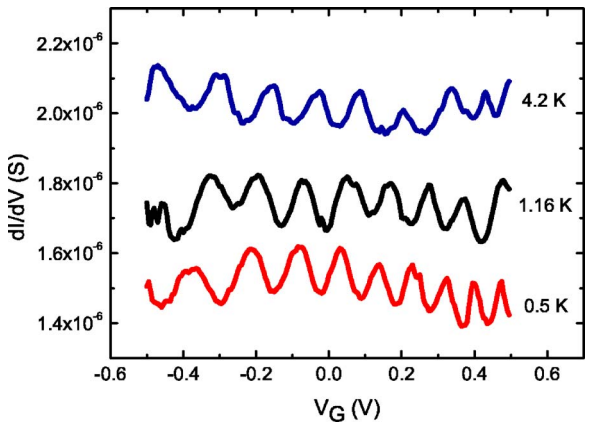

FIG. 4. (Color online) The differential conductance plotted against back-gate voltages measured at 0.5, 1.16, and 4.2 K between electrodes 2 and 3, displaying the periodic CB oscillations.

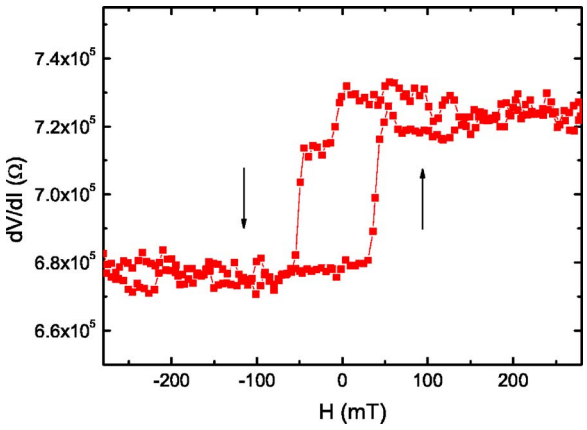

FIG. 5. (Color online) The differential resistance (dV/dI) between electrodes 2 and 3 vs magnetic field with a bias voltage of 5 mV at 0.5 K. A hysteretic switch appears and the dV/dI changes abruptly at the magnetic field of about ±50 mT approximating to the coercive field of the Co film. Out of the hysteretic region, the dV/dI values of positive magnetic fields are larger than those of negative magnetic fields.

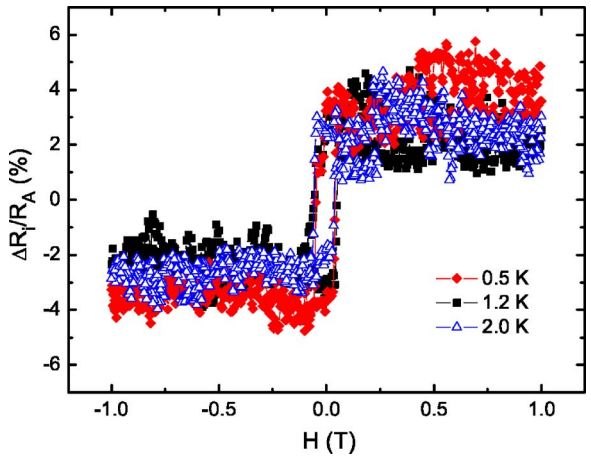

FIG. 6. (Color online) The $\Delta R_i/R_A$ as a function of the external magnetic fields ranging from −1 to 1 T between electrodes 2 and 3 at different temperatures. The relative changes of the differential resistance are around 3.5%, 2.5%, and 2.3% at 0.5, 1.2, and 2 K at the coercive field, respectively.

magnet applied parallel to the SWNT axis directed in the plane of the substrate. Figure 5 shows the two-probe dV/dI as a function of magnetic field with a bias voltage of 5 mV at 0.5 K. We observe a hysteretic and asymmetric differential resistance in the vicinity of zero magnetic field. The change in the differential resistance with magnetic fields mainly appears at ±50 mT, which is commensurate with the coercive field strength of a thin Co film.[20] The average Co domain size is about 50 nm and the diameter of the SWNT is approximately 1.5 nm. The SWNT is in contact with only one or a few magnetic domains in the Co electrode. This indicates that the hysteretic MR should be related to the occurrence and switching of the magnetic domains coupled to the nanotube. It is noteworthy that the differential resistances for positive fields are larger than the differential resistances for negative fields with a pronounced relative change of up to 7%, when the applied magnetic field is above the coercive field. Compared with the case within the coercive fields, the dependence of the differential resistance on magnetic field is relatively weak. We define the differential resistance dV/dI at each magnetic field as R_i, and their relative change as $\Delta R_i/R_A=(R_i-R_A)/R_A$, where R_A is the average value of R_i and ΔR_i is the difference of the differential resistance relative to R_A. Figure 6 shows the $\Delta R_i/R_A$ as a function of magnetic field at the temperatures of 0.5, 1.2, and 2.0 K with a bias voltage of 5 mV. The asymmetric and hysteretic MR remains present even if the scanning range of the magnetic field is extended to 1 T. $\Delta R_i/R_A$ shows the temperature dependence changing from about 2.2% to 3.5% at the coercive field, and the magnitudes are comparable to the common results of tunneling MR in a carbon nanotube connected by two ferromagnetic terminals.

In the hybrid system, the ferromagnetic Co electrode is used as a source of spin-polarized electrons, which have a preferred spin direction determined by an external magnetic field. On the other hand, as a result of size quantization, a SWNT quantum dot has a set of discrete levels with spin degeneracy at small magnetic fields and without considering the spin-orbit interaction. Thus, it seems to be a simple picture that electrons with a preferred spin direction are injected into a SWNT quantum dot through a tunneling barrier driven by a bias voltage, where the tunneling barrier has been considered as an effective means of spin injection.[1] However, the measured MR behavior has never been observed in previous devices consisting of ferromagnetic electrode–carbon nanotube–nonmagnetic metal electrode.[9,15] Owing to the absence of the spin-valve mechanism, it is commonly impossible to obtain the behavior of hysteretic MR in this asymmetric hybrid system. The present MR curves are also different from that of the anisotropic MR of a single ferromagnetic Co film, which is symmetric when the Co film is fully magnetized at opposite fields as great as ±1 T.[21] Also, the SWNT does not have an obvious intrinsic MR, which is confirmed by our measurements of the SWNT coupled to two nonmagnetic metal electrodes. Further, asymmetric MR curves cannot yet be interpreted as the injection of spin-up or spin-down electrons into a SWNT quantum dot with a set of spin-degenerate discrete levels in that tunneling through the system for the case of spin-up and spin-down electrons is equivalent and could not give rise to the observed behaviors. To our knowledge, there is no existing theoretical model that is able to explain our observed hysteretic and asymmetric MR in the SWNT with a single ferromagnetic terminal.

It is well known that the two-probe differential conductance dI/dV, which is the reciprocal of the differential resistance, measured on a SWNT with tunneling contacts gives information about the density of states in the SWNT. The change in the differential resistances in opposite magnetization orientations reflects the different DOSs in the SWNT quantum dot available for the injected spin-up and spin-down electrons. Hence, we presume that the variation in the differential resistance for electrons being injected with opposite spins is due to the existence of the spin-split DOS in the SWNT quantum dot. The energy required in the tunneling process of electrons is different for spin-up and spin-down

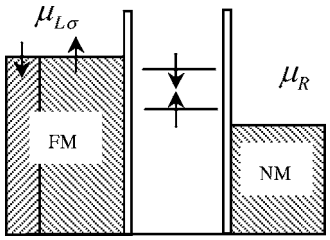

FIG. 7. Schematic diagram of a SWNT quantum dot coupled to a ferromagnetic metal (FM) and a nonmagnetic metal (NM) electrode. The central region denotes the SWNT quantum dot with the spin-split discrete levels, whose spin polarizations are indicated by arrows in the quantum dot region.

states of the SWNT quantum dot. The spin-up and spin-down electrons will have different transmission probabilities due to the spin splitting of energy levels within a finite energy window (bias voltage). One likely source of spin splitting is the spin-orbit interaction in chiral carbon nanotubes, whose chains of carbon atoms spiral around the nanotube axis. The spin-orbit interaction can lift the spin degeneracy, depending on the lattice symmetry. For a finite-length chiral carbon nanotube, a series of discrete levels will be spin split, which is caused by the spin-orbit interaction due to the lack of inversion symmetry.[22]

We model the system of a quantum dot with spin-split levels coupled to a ferromagnetic and a nonmagnetic metal electrode (see Fig. 7) with the Anderson Hamiltonian:

$$H = H_F + H_d + H_N + H_T, \tag{1}$$

where

$$H_F = \sum_{k\sigma} (\varepsilon_k^L - \sigma M) a_{k\sigma}^\dagger a_{k\sigma} = \sum_{k\sigma} \varepsilon_{k\sigma}^L a_{k\sigma}^\dagger a_{k\sigma}, \tag{2}$$

$$H_N = \sum_{k\sigma} \varepsilon_k^R b_{k\sigma}^\dagger b_{k\sigma}, \tag{3}$$

$$H_d = \sum_{\sigma} \varepsilon_{c\sigma} c_{k\sigma}^\dagger c_{k\sigma} + U_c c_\uparrow^\dagger c_\uparrow c_\downarrow^\dagger c_\downarrow, \tag{4}$$

$$H_t = \sum_{k\sigma} L_k a_{k\sigma}^\dagger c_\sigma + \sum_{k\sigma} R_k b_{k\sigma}^\dagger c_\sigma + \text{H.c.} \tag{5}$$

Here H_F is the Hamiltonian of the ferromagnetic electrode with different magnetization orientations due to the reversed external magnetic fields. H_N is the Hamiltonian of the noninteracting nonmagnetic metallic electrode. $a_{k\sigma}^\dagger$ ($a_{k\sigma}$) and $b_{k\sigma}^\dagger$ ($b_{k\sigma}$) are the creation (annihilation) operators for electrons in the ferromagnetic and nonmagnetic metallic electrode, respectively. k and σ are the electron momentum quantum number and the spin index, respectively. H_d models the quantum dot with two levels having different spin orientations with charging energy U_c. H_t describes the tunneling Hamiltonian coupling between the leads and quantum dot region, where L_k and R_k are the hopping matrix elements. The electron current J_σ for the spin component σ is given by the formula based on the Keldysh nonequilibrium Green's function formalism:[23,24]

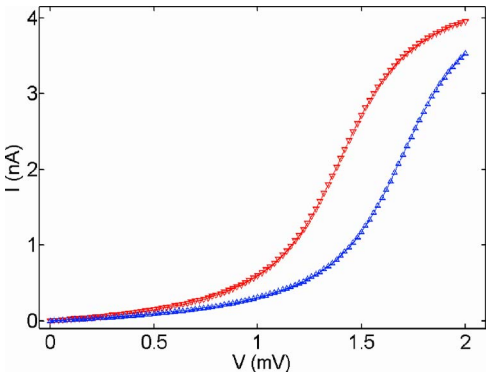

FIG. 8. (Color online) Current-voltage characteristics for the cases that the ferromagnetic electrode is fully magnetized in opposite directions. The tunneling current of spin-down electrons represented by the downward triangle has a higher value than that of spin-up electrons represented by the downward triangle at the same bias voltage.

$$J_\sigma = \frac{1}{\hbar} \int d\varepsilon [f_\sigma^L(\varepsilon) - f^R(\varepsilon)] \frac{\Gamma_\sigma^L \Gamma^R}{\Gamma_\sigma^L + \Gamma^R} \left(-\frac{1}{\pi} \text{Im}\, G_{\sigma\sigma}^r(\varepsilon) \right], \tag{6}$$

where $f_\sigma^L(\varepsilon) = [\exp(\varepsilon - \mu_{L\sigma})/k_B T + 1]^{-1}$ and $f_\sigma^R(\varepsilon) = [\exp(\varepsilon - \mu_R)/k_B T + 1]^{-1}$ are the Fermi-Dirac distribution functions of electrons in the ferromagnetic and nonmagnetic metallic electrodes with spin index σ. $\Gamma_\sigma^L = (1 + \sigma P)\Gamma^L$, where P is the polarization of ferromagnetic electrode. Γ^L and Γ^R are the linewidth functions. $G_{\sigma\sigma}^r(\varepsilon)$ is the retarded Green's function given by the Fourier transform of $G_{\sigma\sigma}^r(t)$, which is defined as $G_{\sigma\sigma}^r(t) = -i\theta(t)\langle [c_\sigma(t), c_\sigma^\dagger(0)] \rangle$. The retarded Green's function $G_{\sigma\sigma}^r(\varepsilon)$ can be solved by the standard equation of motion technique:[23,25]

$$G_{\sigma\sigma}^r(\varepsilon) = \frac{\varepsilon - \varepsilon_{c\sigma} - U_c(1-n)}{(\varepsilon - \varepsilon_{c\sigma})(\varepsilon - \varepsilon_{c\sigma} - U_c) - (-i/2\Gamma)[\varepsilon - \varepsilon_{c\sigma} - U_c(1-n)]}, \tag{7}$$

where $\Gamma = \Gamma_\sigma^L + \Gamma^R$, and n is the electron occupation number at the spin-σ state in the quantum dot which is calculated by the self-consistent method. The process follows the detailed derivation in Refs. 26 and 27.

For simplicity, we consider the special case that the ferromagnetic lead is fully polarized and set $\Gamma_\sigma^L = \Gamma^R = \Gamma/2$, and $\Gamma = 0.5$ with meV as the energy unit. The charging energy U_c of the SWNT quantum dot is fixed to be 1.85 for the tube length 370 nm and we presume two spin-split levels of the quantum dot $\varepsilon_{c\uparrow} = 0.3$, $\varepsilon_{c\downarrow} = 0.6$ at the low temperature $k_B T = 0.03$, although the precise estimation is not known. In this description, Fig. 8 is the plot of the current-voltage curves at opposite spin-polarized situations of the ferromagnetic electrode. It can be seen at the same low bias voltage that the tunneling current of the spin-down electrons is larger than that of the spin-up electrons, which is qualitatively in agreement with the present experimental observation. On the

contrary, if the quantum dot has spin-degenerate levels in the hybrid device, then the variation in resistance does not occur with the reversal of magnetization direction at a finite bias voltage.

In summary, transport measurements were performed in a hybrid system of ferromagnetic metal electrode–SWNT–nonmagnetic metal electrode. At significantly low temperature, the differential conductance shows suppression of the zero-bias conductance and the CB oscillations. Hysteretic and asymmetric characteristics of the differential resistance are found by sweeping the magnetic field. This anomalous MR can be interpreted by the spin-dependent transport through the SWNT quantum dot with the spin-split DOS. The spin-orbit interaction in chiral nanotubes is one possible source of the spin splitting.

This work is supported by the Knowledge Innovation Program of CAS and the NSFC.

[1] S. A. Wolf, D. D. Awschalom, R. A. Buhrman, J. M. Daughton, S. von Molnęr, M. L. Roukes, A. Y. Chtchelkanova, and D. M. Treger, Science **294**, 1488 (2001).
[2] I. Žutić, J. Fabian, and S. D. Sarma, Rev. Mod. Phys. **76**, 323 (2004).
[3] K. Tsukagoshi, B. W. Alphenaar, and H. Ago, Nature (London) **401**, 572 (1999).
[4] S. Chakraborty, K. M. Walsh, B. W. Alphenaar, Lei Liu, and K. Tsukagoshi, Appl. Phys. Lett. **83**, 1008 (2003).
[5] S. Sahoo, T. Kontos, and C. Schönenberger, Appl. Phys. Lett. **86**, 112109 (2005).
[6] J. R. Kim, H. M. So, J. J. Kim, and J. Kim, Phys. Rev. B **66**, 233401 (2002).
[7] M. Jullière, Phys. Lett. **54A**, 225 (1975).
[8] H. Mehrez, Jeremy Taylor, Hong Guo, Jian Wang, and Christopher Roland, Phys. Rev. Lett. **84**, 2682 (2000).
[9] B. W. Alphenaar, K. Tsukagoshi, and M. Wagner, J. Appl. Phys. **89**, 6863 (2001).
[10] A. Jensen, J. R. Hauptmann, J. Nygård, and P. E. Lindelof, Phys. Rev. B **72**, 035419 (2005).
[11] B. Zhao, I. Mönch, T. Mühl, H. Vinzelberg, and C. M. Schneider, J. Appl. Phys. **91**, 7026 (2002).
[12] B. Zhao, I. Mönch, H. Vinzelberg, T. Mühl, and C. M. Schneider, Appl. Phys. Lett. **80**, 3144 (2002).
[13] S. J. Tans, M. H. Devoret, H. Dai, A. Thess, R. E. Smalley, L. J. Geerligs, and C. Dekker, Nature (London) **386**, 474 (1997).
[14] M. Bockrath, D. H. Cobden, P. L. McEuen, N. G. Chopra, A. Zettl, A. Thess, and R. E. Smalley, Science **275**, 1922 (1997).
[15] S. Sahoo, T. Kontos, J. Furer, C. Hoffmann, M. Gräber, A. Cottet, and C. Schönenberger, Nat. Phys. **1**, 99 (2005).
[16] B. Nagabhirava, T. Bansal, G. U. Sumanasekera, B. W. Alphenaar, and L. Liu, Appl. Phys. Lett. **88**, 023503 (2006).
[17] L. W. Liu, J. H. Fang, L. Lu, Y. J. Ma, Z. Zhang, H. F. Yang, A. Z. Jin, and C. Z. Gu, J. Phys. Chem. B **108**, 18460 (2004).
[18] W. J. Liang, M. Bockrath, D. Bozovic, J. H. Hafner, M. Tinkham, and Hongkun Park, Nature (London) **411**, 665 (2001).
[19] J. Nygård, D. H. Cobden, M. Bockrath, P. L. McEuen, and P. E. Lindelof, Appl. Phys. A: Mater. Sci. Process. **69**, 297 (1999).
[20] U. Rüdiger, J. Yu, L. Thomas, S. S. P. Parkin, and A. D. Kent, Phys. Rev. B **59**, 11914 (1999).
[21] M. Viret, D. Vignoles, D. Cole, J. M. D. Coey, W. Allen, D. S. Daniel, and J. F. Gregg, Phys. Rev. B **53**, 8464 (1996).
[22] L. Chico, M. P. López-Sancho, and M. C. Muñoz, Phys. Rev. Lett. **93**, 176402 (2004).
[23] A. Groshev, T. Ivanov, and V. Valtchinov, Phys. Rev. Lett. **66**, 1082 (1991).
[24] Y. Meir and N. S. Wingreen, Phys. Rev. Lett. **68**, 2512 (1992).
[25] W. Long, Q. F. Sun, H. Guo, and J. Wang, Appl. Phys. Lett. **83**, 1397 (2003).
[26] Y. Meir, N. S. Wingreen, and P. A. Lee, Phys. Rev. Lett. **70**, 2601 (1993).
[27] Q. F. Sun and H. Guo, Phys. Rev. B **66**, 155308 (2002).